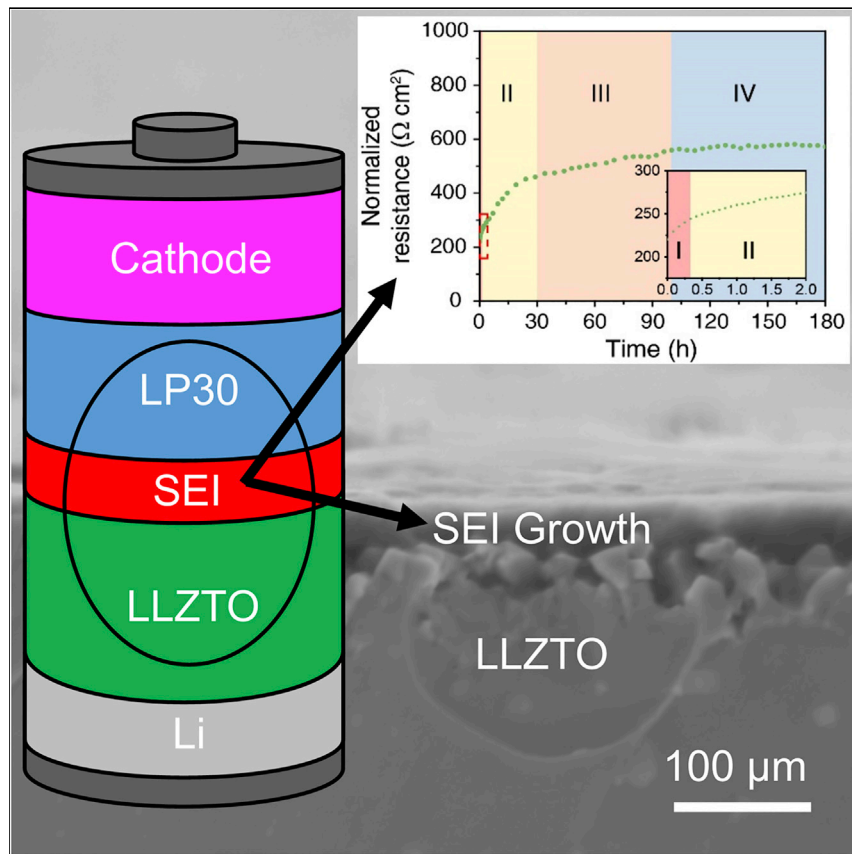


Report

The Interface between $\text{Li}_{6.5}\text{La}_3\text{Zr}_{1.5}\text{Ta}_{0.5}\text{O}_{12}$ and Liquid Electrolyte



Improved battery energy densities could be achieved by utilizing lithium metal anodes. Liquid electrolytes are incompatible with lithium, and solid electrolyte replacements have been hindered by cathode interface challenges. A hybrid cell, employing a solid electrolyte to separate lithium from liquid catholyte, could mitigate these issues. However, here we show that the interface between LP30 liquid electrolyte and a garnet solid electrolyte is a significant source of resistance and reveal the formation and composition of a resulting interphase layer.

Jingyuan Liu, Xiangwen Gao,
Gareth O. Hartley, ..., Alex W.
Robertson, Lee R. Johnson,
Peter G. Bruce

lee.johnson@nottingham.ac.uk (L.R.J.)
peter.bruce@materials.ox.ac.uk (P.G.B.)

HIGHLIGHTS

Solid electrolytes could be used to protect lithium anodes in liquid cells

The LLZTO/LP30 interface has a significant associated resistance

An interphase develops at the interface

The interphase contains LiF , Li_2CO_3 , LiO_2 , and organic species

Report

The Interface between $\text{Li}_{6.5}\text{La}_3\text{Zr}_{1.5}\text{Ta}_{0.5}\text{O}_{12}$ and Liquid Electrolyte

Jingyuan Liu,^{1,2,6} Xiangwen Gao,^{1,6} Gareth O. Hartley,^{1,6} Gregory J. Rees,¹ Chen Gong,¹ Felix H. Richter,³ Jürgen Janek,³ Yongyao Xia,² Alex W. Robertson,¹ Lee R. Johnson,^{4,*} and Peter G. Bruce^{1,5,7,*}

SUMMARY

An advantageous solid electrolyte/liquid electrolyte interface is crucial for the implementation of a protected lithium anode in liquid electrolyte cells. $\text{Li}_{6.5}\text{La}_3\text{Zr}_{1.5}\text{Ta}_{0.5}\text{O}_{12}$ (LLZTO) garnet electrolytes are among the few solid electrolytes that are stable in contact with lithium metal. We show LLZTO is unstable in contact with the organic carbonate-based Li^+ liquid electrolyte used in conventional Li-ion cells. The interfacial resistance between LLZTO and LiPF_6 in $(\text{CH}_2\text{O})_2\text{CO}$: $\text{OC}(\text{OCH}_3)_2$ (1:1 v/v) increases with time due to the growth of a lithium-ion-conducting solid electrolyte interphase (SEI) at the surface of the ceramic electrolyte. The interphase is composed of Li_2CO_3 , LiF , Li_2O , and organic carbonates. Even at a rate of 5 mA cm^{-2} , a 3 V potential drop occurs across the LLZTO/liquid electrolyte interface. A practical LLZTO membrane (thickness $\sim 10 \mu\text{m}$), in contact with a lithium anode, gives a potential loss of $\sim 16 \text{ mV}$, less than 1% of the resistance of the SEI.

INTRODUCTION

The renaissance of interest in Li^+ -conducting ceramic electrolytes has been driven by two applications: their use in solid-state batteries and as protective membranes for lithium metal electrodes in liquid electrolyte cells. The latter application would allow graphitic anodes to be replaced with lithium in conventional lithium-ion batteries and would enable lithium-metal anodes to be used in Li-S and Li-O₂ batteries.^{1–7} In contrast to graphite electrodes, it is difficult and conceivably impossible, to operate a lithium-metal anode in direct contact with a liquid electrolyte because the solid electrolyte interphase (SEI) is not stable, this results in cycling inefficiency and safety problems.^{1,3,8} As a result, considerable effort has been placed on developing all-solid-state batteries, in which the liquid electrolyte is replaced with a solid electrolyte. However, the composite cathode/solid electrolyte interface present in all-solid-state batteries has been plagued by capacity fading due to electrochemical instability, volume expansion, and contact loss issues.^{9,10} Addition of liquid electrolytes to wet the cathode has been proposed; with this approach, the anode challenges of a liquid battery are separated from the largely unsolved cathode challenges currently hindering solid-state batteries.^{4,11,12} In theory, this would enable a metal anode to be employed while using effective existing liquid catholytes. While much attention has been devoted to the challenges that face the lithium/solid electrolyte interface, relatively little attention has been paid to the interface between ceramic and liquid electrolytes, yet this interface is crucial for the successful implementation of a protected lithium anode in a liquid electrolyte cell, especially in Li-O₂ and Li-S batteries.^{4,7,12–15} Pioneering work has suggested that at the solid electrolyte/liquid electrolyte (SE/LE) interface, Li^+ ions are exchanged across the

Context & Scale

The need for improved electrical energy storage has generated intense interest in the challenges that hinder going beyond today's lithium-ion battery technology, which will require lithium metal to be used as an anode. However, lithium reacts with liquid electrolytes, and it is now widely accepted that the lithium anode may need to be protected by a solid electrolyte membrane.

$\text{Li}_{6.5}\text{La}_3\text{Zr}_{1.5}\text{Ta}_{0.5}\text{O}_{12}$ (LLZTO) is one of the few solid electrolytes that are stable in contact with lithium metal, and as such, it is an attractive candidate for protecting the lithium metal anode. Here, we show that LLZTO is not stable in contact with the carbonate-based liquid electrolyte currently used in commercial lithium-ion batteries (1 M LiPF_6 in ethylene carbonate: dimethyl carbonate [1:1 v/v]). Consequently, the resistance between the ceramic and liquid electrolyte increases to undesirable values due to the formation of a solid electrolyte interphase.

interface generating a junction potential, with the kinetics of exchange being determined by the processes of Li^+ desolvation, adsorption on the ceramic surface and incorporation into the lattice.^{13–15} However, recent studies indicate that the processes are more complex and can give rise to high impedances.^{4,9–12} The resistance at the SE/LE interface of a protected lithium anode can introduce a significant internal resistance to the cell, representing a major barrier to the implementation of such anodes.⁴ Thus, the challenges associated with this interface are as important as those at the lithium metal/solid electrolyte interface.

Previous studies of the SE/LE interface have investigated $\text{La}_{0.55}\text{Li}_{0.35}\text{TiO}_3$ ^{13–15} and $\text{Li}_{1+x}\text{Al}_x\text{Ge}_{2-x}(\text{PO}_4)_3$.⁴ However, neither of these ceramic electrolytes is likely to be used in practical cells due to issues resulting from the reactivity between the ceramic and the lithium metal.^{16–19} Of the solid electrolytes under investigation today, those of the garnet family, typified by $\text{Li}_{6.5}\text{La}_3\text{Zr}_{1.5}\text{Ta}_{0.5}\text{O}_{12}$ (LLZTO), are the most thermodynamically stable in contact with lithium metal and are widely regarded as very promising electrolytes for practical lithium anode protective membranes.^{20–23} Therefore, it is important to study the interface between the garnet-type solid electrolytes and the aprotic liquid electrolytes used in lithium-ion cells. Here we investigate the interface between LLZTO and the liquid electrolyte LP30 (LiPF_6 in ethylene carbonate: dimethyl carbonate [DMC] [1:1 v/v]), the typical liquid electrolyte used in Li-ion cells. The impedance of the LLZTO/LP30 interface increases with time due to the growth of an interphase containing Li_2O , LiF , PF_y , and Li_2CO_3 . The interfacial impedance stabilizes at $\sim 580 \Omega \text{ cm}^2$ after 150 h; at a current density of 5 mA cm^{-2} , this resistance introduces a potential drop across a SE/LE interface of $\sim 3 \text{ V}$, which is unacceptably large for a cell with an open circuit potential between 3–4 V. These results demonstrate that mitigating reactions that lead to unacceptable resistance at the SE/LE interface will be critical to the development of cells employing protected lithium anodes.

RESULTS AND DISCUSSION

An LLZTO disk was prepared by the modified Pechini sol-gel method outlined in the [Supplemental Information](#). Powder X-ray diffraction and Fourier transform infrared (FTIR) spectroscopy showed no evidence of impurities after surface cleaning ([Figures S1 and S2](#)). The LLZTO disk was introduced into a 4-electrode cell, where it separated two compartments filled with LP30 electrolyte (BASF battery-grade; $\text{H}_2\text{O} < 15 \text{ ppm}$, $\text{HF} < 50 \text{ ppm}$). Electrochemical impedance spectroscopy (EIS) was then performed in a 4-electrode configuration to investigate Li^+ transport across the interface between LLZTO and LP30 ([Figure S3A](#)). The use of two reference electrodes (REs) eliminates impedance contributions from the current carrying electrodes (CCEs), leaving only the response from the ceramic, the liquid electrolyte, and the interface between them.^{4,13,14} The respective impedance contributions are assigned in [Figures S3B](#) and [S4](#) with corresponding values shown in [Table S1](#); here, we focus on the resistance ($R_{\text{SE/LE}}$) and capacitance ($C_{\text{SE/LE}}$) values for the SE/LE interface.⁴ The variation of $R_{\text{SE/LE}}$ and $C_{\text{SE/LE}}$ with time, is shown in [Figure 1](#). The interfacial resistance increases with time as shown in [Figure 1A](#), which indicates that the SE/LE interface is not stable and undergoes change. The variation of $R_{\text{SE/LE}}$ with time can be divided into four regions. Starting with region III (30–100 h), $R_{\text{SE/LE}}$ increases by $\sim 22\%$ ([Figure 1A](#)) whereas $C_{\text{SE/LE}}$ decreases by $\sim 23\%$ over the same period ([Figure 1B](#)). An ionically conducting layer on the SE surface that increases in thickness with time would lead to such dependence, as the resistance and capacity are respectively proportional and inversely proportional to the layer thickness, $R \propto \rho l/A$ and $C \propto \epsilon A/l$, where ρ is the resistivity and ϵ is the electric constant; A is the area of the layer and l is the thickness.

¹Departments of Materials and Chemistry, University of Oxford, Parks Road, Oxford OX1 3PH, UK

²Department of Chemistry and Shanghai Key Laboratory of Molecular Catalysis and Innovative Materials, Institute of New Energy, iChEM (Collaborative Innovation Center of Chemistry for Energy Materials), Fudan University, Shanghai 200433, China

³Physikalisch-Chemisches Institut & Center for Materials Research, Justus-Liebig-Universität Giessen, Heinrich-Buff-Ring 17, Giessen 35392, Germany

⁴School of Chemistry and GSK Carbon Neutral Laboratory for Sustainable Chemistry, University of Nottingham, Jubilee Campus, Nottingham NG7 2TU, UK

⁵The Faraday Institution, Harwell Campus, Didcot OX11 0RA, UK

⁶These authors contributed equally

⁷Lead Contact

*Correspondence:

lee.johnson@nottingham.ac.uk (L.R.J.), peter.bruce@materials.ox.ac.uk (P.G.B.)

<https://doi.org/10.1016/j.joule.2019.10.001>

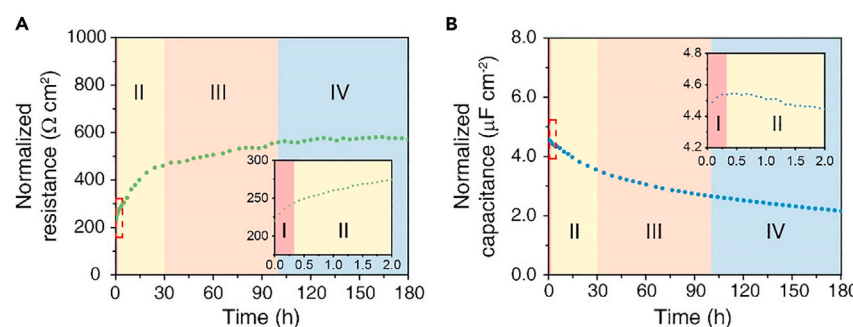


Figure 1. Electrochemical Impedance Behaviour of the LLZTO/LP30 Interface with Time as Determined by Electrochemical Impedance Spectroscopy

(A) Interfacial resistance ($R_{\text{SE/LE}}$) with time.

(B) Interfacial capacitance ($C_{\text{SE/LE}}$) with time.

The time dependence is divided into four regions, I, II, III, and IV, corresponding to different trends. Insets show the changes in the initial 2 h. All values have been normalized by the surface area of one SE/LE interface of the symmetrical cell.

In the initial 30 h, two $R_{\text{SE/LE}}$ regions are observed, region I (0–20 min) and region II (20–30 h). At the start of region I, the initial resistance is $220 \Omega \text{ cm}^2$, suggesting that even within the timescale of our first impedance measurement after cell assembly, typically 5 min, a significant resistance has built up. In region I, the capacitance and resistance rise by 2% and 10%, respectively. We interpret the rise of capacitance as a result of liquid electrolyte ingress into the pores/grain boundaries near the surface, leading to an increase in the effective contact area between the liquid and solid electrolyte and hence an increase in $C_{\text{SE/LE}}$. Despite the increased interfacial area, the initial $220 \Omega \text{ cm}^2$ resistance and the increasing resistance in region I, indicate that Li^+ exchange across the interface is already being inhibited, which suggests a reaction is already taking place between the liquid electrolyte and the surface of LLZTO. Over region II (20 min to 30 h), the resistance increases by a further ~90% and the capacitance decreases by ~25%, indicating that there is now a significant barrier to Li^+ transport.

To explore the formation of the interphase over these regions, LLZTO disks were removed from the liquid electrolyte and were washed in DMC by dipping to minimize contamination of the SEI due to the precipitation of electrolyte salts; the disk surfaces were then analyzed using a scanning electron microscope (SEM), with all transfers being performed without exposure to air. Top-down view SEM images of the LLZTO surface following 2 h of exposure to LP30 (Figure S5B) show that the surface remains somewhat characteristic of a pristine ceramic, with striations from the initial polishing clearly being seen across the entire surface. In the cross-sectional view, morphological changes indicative of liquid electrolyte ingress into the surface can be seen after 2 h, (Figure 2Aii). Cross-sectional SEM images taken over region II indicate that the LLZTO disk reacts with LP30 and a continuous and morphologically distinct interphase with an average thickness of 350 nm ($\sigma = 190 \text{ nm}$) is established after 30 h (Figure 2Aiii). The development of the surface layer is also observed in top-down view images, (Figures S5C and S5D). Over region III, the interphase thickens (Figures S5E and S5F) and after 100 h, the interphase has an average thickness of 420 nm ($\sigma = 120 \text{ nm}$) (Figure 2Aiv).

To analyze the interphase at early stages, high-resolution transmission electron microscopy (HRTEM) was performed on LLZTO particles following exposure to LP30 for 10 h (Figure S6); this revealed that LLZTO particles became embedded inside a relatively amorphous layer, confirming the formation of a SEI. Inspection of the interphase at increased magnification revealed the presence of small crystallites in

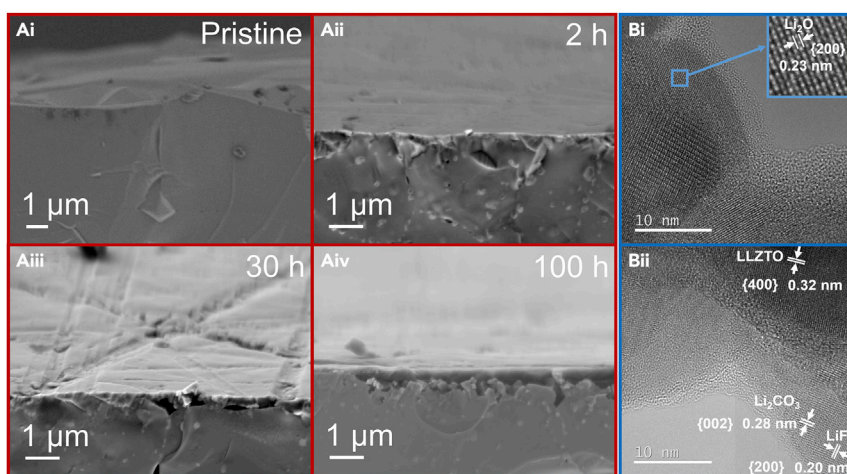


Figure 2. Electron Micrographs Showing the Development of an Interphase between LLZTO and LP30

(A) SEM images of cross-sectioned LLZTO disks after immersion in LP30 electrolyte for various times.

(B) HRTEM images of LLZTO particles following exposure to LP30 for 10 h and after washing with DMC, showing (i) Li_2O {200} with an interlayer spacing of 0.23 nm and (ii) Li_2CO_3 {002} and LiF {200}.

the outer layer with lattice spacing consistent with the crystal structures of antifluorite cubic Li_2O , monoclinic Li_2CO_3 , and face-centered cubic LiF , respectively (Figures 2Bi and 2Bii).^{24–26}

X-ray photoelectron spectroscopy (XPS), time of flight secondary ion mass spectrometry (TOF-SIMS), solid-state magic angle spinning (MAS), nuclear magnetic resonance (NMR) experiments, and FTIR spectroscopy were used to characterize the interphase. Li 1s XPS spectra shift to more positive binding energies upon exposure to LP30, indicating interfacial Li^+ is in a different chemical environment to that of bulk LLZTO (Figure S7). F 1s spectra show the presence of LiF , LiPF_6 , and PF_y compounds in the surface film, (Figure 3).²⁷ The LiPF_6 was not fully removed by washing and is likely to be embedded in the surface film. The LiF and PF_y must originate from decomposition of the LiPF_6 salt. Further evidence of the presence of LiF and LiPF_6 in the SEI was provided by ex situ ^{19}F MAS NMR (Figure S8). O 1s and C 1s XPS (Figure 3) indicates that the surface layer contains Li_2O , CO_3^{2-} , and Li-O-C .^{28–31} TOF-SIMS was performed on the disk after immersion in LP30 for 150 h (Figure S9) ZrO^- fragments were detected with a relatively low intensity at the surface of the disk after 150 h of exposure; the intensity of ZrO^- is indicative of the relative concentration of LLZTO. In agreement with the XPS results, LiF^- and LiCO_3^- fragments show relatively high intensities close to the disk surface, confirming the presence of an SEI rich in LiF and Li_2CO_3 . Furthermore, TOF-SIMS clearly identifies the presence of organic decomposition fragments, confined to the outer region nearer to the LE/SEI interface, and it was further observed by FTIR spectroscopy, showing the presence of peaks for Li_2CO_3 at $1,500 \text{ cm}^{-1}$ (Figure S2). Additionally, small peaks are present around $1,750 \text{ cm}^{-1}$ in the carbonyl group region which likely correspond to both solvent decomposition and organic carbonates originating from the LP30 electrolyte and DMC used for washing.

The effect of the SE/LE interface on cell performance was examined by cycling at a current density of 0.1 mA cm^{-2} (Figure 4) using the 4-electrode cell shown in Figure S3A. The total polarization observed during cycling is due to the combined

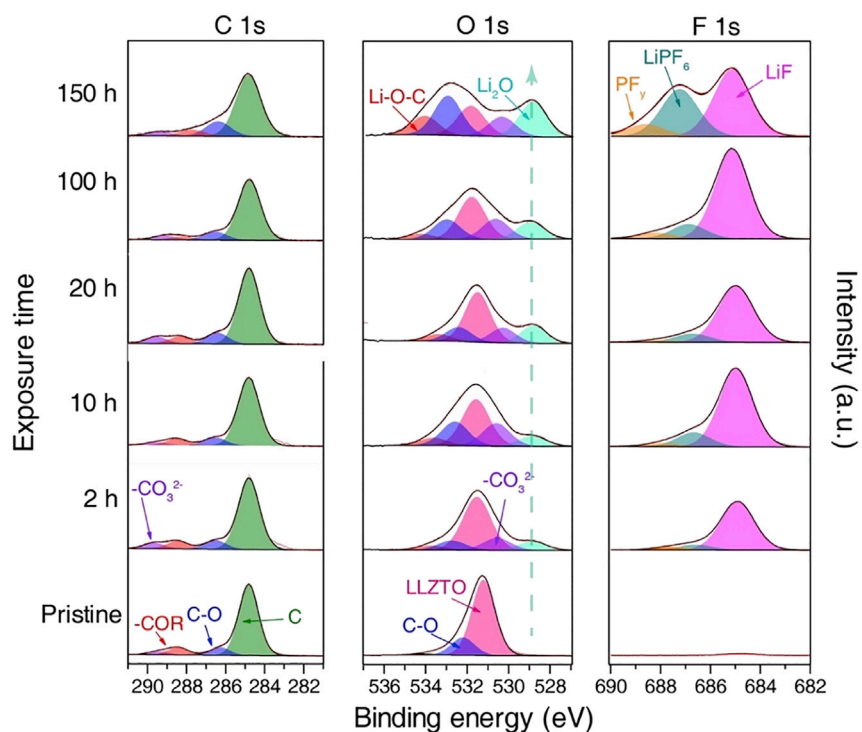


Figure 3. C 1s, O 1s, and F 1s XPS Spectra of LLZTO Disks after Exposure to LP30 for 0, 2, 10, 20, 100, and 150 h

resistance of LP30 in both halves of the cell, as well as the LLZTO disk and the two SE/LE interfaces from the respective sides of the LLZTO disk. During the early stages of cycling, the voltage polarization increased from 0.12 V at $t = 0$ to 0.19 V, corresponding to a resistance increase of $700 \Omega \text{ cm}^2$. This increase was primarily due to changes in the two respective SE/LE interfaces, such that the resistance of an individual SE/LE interface effectively increased by $350 \Omega \text{ cm}^2$. This result is consistent with the resistance of the SE/LE interface, $360 \Omega \text{ cm}^2$, seen in Figure 1A, and is due to the formation of the SEI.

Dissimilar from the 4-electrode studies here, in a practical cell, the polarization comes from the combined resistance of the solid electrolyte, one lithium/SE interface, and one SE/LE interface. A ceramic LLZTO membrane with a thickness of 10 μm would have a total resistance of $\sim 1.2 \Omega \text{ cm}^2$ and according to previous studies, the interfacial resistance between lithium metal and garnet-type solid electrolytes could be as low as $\sim 2 \Omega \text{ cm}^2$.³² The combination of these resistances indicates that introducing an LLZTO membrane to protect lithium anode could result in a resistance of $\sim 3.2 \Omega \text{ cm}^2$. As a practical cell would need to operate at a current density of 5 mA cm^{-2} , a potential drop of $\sim 16 \text{ mV}$ would be incurred. However, according to our studies, one LLZTO/LE interface has a total resistance of $\sim 580 \Omega \text{ cm}^2$, and therefore, the potential drop across this interface is expected to be $\sim 3 \text{ V}$, which is almost 200 times larger than the combined resistance of the solid electrolyte and the lithium/SE interface; this is unacceptably large for practical applications.

Conclusions

Garnets, such as LLZTO, appear to be stable in contact with lithium metal and are therefore attractive candidates as protecting membranes for the lithium metal anode. Here, we show that LLZTO is not stable in contact with a typical lithium-ion organic carbonate

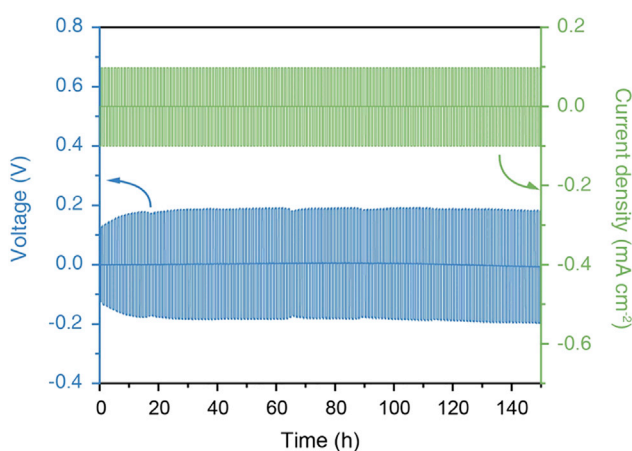


Figure 4. Galvanostatic Cycling of an LLZTO Disk (~2.5 mm Thickness) with LP30 in a 4-Electrode Cell at a Current Density of 0.1 mA cm^{-2}

The 4-electrode cell has two LLZTO/LE interfaces.

electrolyte, LP30. The interfacial resistance grows with time due to the growth of a lithium-ion-conducting solid electrolyte interphase formed by a reaction between the ceramic electrolyte and the liquid electrolyte. The interphase is predominantly composed of LiF, together with Li_2O , Li_2CO_3 , and decomposition fragments. The formation and growth of such a layer has important implications for the use of LLZTO in cells with liquid electrolytes, as it would introduce a significant resistance during cycling. These results indicate that understanding the solid/liquid electrolyte interface is just as important as understanding the solid/solid interface of a protected lithium anode. As such, strategies will be needed to inhibit the formation of these highly resistive SEIs if metallic lithium is to be used in beyond lithium-ion batteries.

DATA AND CODE AVAILABILITY

Supporting research data have been deposited in the Oxford Research Archive and are available under this <https://doi.org/10.5287/bodleian:mqmPV0pmD>.

SUPPLEMENTAL INFORMATION

Supplemental Information can be found online at <https://doi.org/10.1016/j.joule.2019.10.001>.

ACKNOWLEDGMENTS

P.G.B. is indebted to the Engineering and Physical Sciences Research Council (EPSRC), including the SUPERGEN Energy Storage Hub (EP/L019469/1) and Enabling Next Generation Lithium Batteries (EP/M009521/1), the University of Oxford experimental equipment upgrade (EP/M02833X/1), the Henry Royce Institute for capital equipment (EP/R010145/1), and the Faraday Institution All-Solid-State Batteries with lithium and sodium Anodes (FIRG007 and FIRG008) for financial support. L.R.J. gratefully acknowledges support from the University of Nottingham's Beacon in Propulsion Futures and the EPSRC (EP/S001611/1). A.W.R. thanks the support of the Royal Society.

AUTHOR CONTRIBUTIONS

J.L., X.G., and G.O.H. designed experiments. J.L. and G.O.H. performed electrochemical measurements, and X.G., C.G., G.J.R., and G.O.H. performed

characterization analysis. J.L., X.G., G.O.H., F.H.R., J.J., Y.X., A.W.R., L.R.J., and P.G.B. interpreted the data. L.R.J. and P.G.B. wrote the paper with contributions from J.L., X.G., and G.O.H.

DECLARATION OF INTERESTS

The authors declare no competing interests.

Received: February 12, 2019

Revised: May 20, 2019

Accepted: October 1, 2019

Published: October 30, 2019

REFERENCES

1. Armand, M., and Tarascon, J.M. (2008). Building better batteries. *Nature* **451**, 652–657.
2. Bruce, P.G., Freunberger, S.A., Hardwick, L.J., and Tarascon, J.M. (2011). $\text{Li}-\text{O}_2$ and Li-S batteries with high energy storage. *Nat. Mater.* **11**, 19–29.
3. Gao, Z., Sun, H., Fu, L., Ye, F., Zhang, Y., Luo, W., and Huang, Y. (2018). Promises, challenges, and recent progress of inorganic solid-state electrolytes for all-solid-state lithium batteries. *Adv. Mater.* **30**, e1705702.
4. Busche, M.R., Drossel, T., Leichtweiss, T., Weber, D.A., Falk, M., Schneider, M., Reich, M.L., Sommer, H., Adelhelm, P., and Janek, J. (2016). Dynamic formation of a solid-liquid electrolyte interphase and its consequences for hybrid-battery concepts. *Nat. Chem.* **8**, 426–434.
5. Gao, X., Chen, Y., Johnson, L.R., Jovanov, Z.P., and Bruce, P.G. (2017). A rechargeable lithium–oxygen battery with dual mediators stabilizing the carbon cathode. *Nat. Energy* **2**, 17118.
6. Aurbach, D., McCloskey, B.D., Nazar, L.F., and Bruce, P.G. (2016). Advances in understanding mechanisms underpinning lithium–air batteries. *Nat. Energy* **1**.
7. Bergner, B.J., Busche, M.R., Pinedo, R., Berkes, B.B., Schröder, D., and Janek, J. (2016). How to improve capacity and cycling stability for next generation $\text{Li}-\text{O}_2$ batteries: approach with a solid electrolyte and elevated redox mediator concentrations. *ACS Appl. Mater. Interfaces* **8**, 7756–7765.
8. Ryou, M.-H., Lee, Y.M., Lee, Y., Winter, M., and Bieker, P. (2015). Mechanical surface modification of lithium metal: Towards improved Li metal anode performance by directed Li plating. *Adv. Funct. Mater.* **25**, 834–841.
9. Zhang, W., Richter, F.H., Culver, S.P., Leichtweiss, T., Lozano, J.G., Dietrich, C., Bruce, P.G., Zeier, W.G., and Janek, J. (2018). Degradation mechanisms at the $\text{Li}_{10}\text{GeP}_2\text{S}_12/\text{LiCoO}_2$ cathode interface in an all-solid-state lithium-ion battery. *ACS Appl. Mater. Interfaces* **10**, 22226–22236.
10. Koerver, R., Aygün, I., Leichtweiß, T., Dietrich, C., Zhang, W., Binder, J.O., Hartmann, P., Zeier, W.G., and Janek, J. (2017). Capacity fade in solid-state batteries: interphase formation and chemomechanical processes in nickel-rich layered oxide cathodes and lithium thiophosphate solid electrolytes. *Chem. Mater.* **29**, 5574–5582.
11. Manthiram, A., Yu, X., and Wang, S. (2017). Lithium battery chemistries enabled by solid-state electrolytes. *Nat. Rev. Mater.* **2**.
12. Xu, B., Duan, H., Liu, H., Wang, C.A., and Zhong, S. (2017). Stabilization of garnet/liquid electrolyte interface using superbase additives for hybrid Li batteries. *ACS Appl. Mater. Interfaces* **9**, 21077–21082.
13. Abe, T., Sagane, F., Ohtsuka, M., Iriyama, Y., and Ogumi, Z. (2005). Lithium-ion transfer at the interface between lithium-ion conductive ceramic electrolyte and liquid electrolyte—a key to enhancing the rate capability of lithium-ion batteries. *J. Electrochem. Soc.* **152**, A2151–A2154.
14. Yamada, Y., Sagane, F., Iriyama, Y., Abe, T., and Ogumi, Z. (2009). Kinetics of lithium-ion transfer at the interface between $\text{Li}_{0.35}\text{La}_{0.55}\text{TiO}_3$ and binary electrolytes. *J. Phys. Chem. C* **113**, 14528–14532.
15. Sagane, F., Abe, T., and Ogumi, Z. (2009). Li^+ -ion transfer through the interface between Li^+ -ion conductive ceramic electrolyte and Li^+ -ion-concentrated propylene carbonate solution. *J. Phys. Chem. C* **113**, 20135–20138.
16. Inaguma, Y., Liquan, C., Itoh, M., Nakamura, T., Uchida, T., Ikuta, H., and Wakihara, M. (1993). High ionic conductivity in lithium lanthanum titanate. *Solid State Commun.* **86**, 689–693.
17. Stramare, S., Thangadurai, V., and Weppner, W. (2003). Lithium lanthanum titanates: a review. *Chem. Mater.* **15**, 3974–3990.
18. Hartmann, P., Leichtweiss, T., Busche, M.R., Schneider, M., Reich, M., Sann, J., Adelhelm, P., and Janek, J. (2013). Degradation of NASICON-type materials in contact with lithium metal: formation of mixed conducting interphases (MCI) on solid electrolytes. *J. Phys. Chem. C* **117**, 21064–21074.
19. Chung, H., and Kang, B. (2017). Mechanical and thermal failure induced by contact between a $\text{Li}_{1.5}\text{Al}_{0.5}\text{Ge}_{1.5}(\text{PO}_4)_3$ solid electrolyte and Li metal in an all solid-state Li cell. *Chem. Mater.* **29**, 8611–8619.
20. Ma, C., Cheng, Y., Yin, K., Luo, J., Sharifi, A., Sakamoto, J., Li, J., More, K.L., Dudney, N.J., and Chi, M. (2016). Interfacial stability of Li metal–solid electrolyte elucidated via *in situ* electron microscopy. *Nano Lett.* **16**, 7030–7036.
21. Nemori, H., Matsuda, Y., Mitsuoka, S., Matsui, M., Yamamoto, O., Takeda, Y., and Imanishi, N. (2015). Stability of garnet-type solid electrolyte $\text{Li}_x\text{La}_3\text{A}_2-y\text{ByO}_{12}$ ($\text{A}=\text{Nb}$ or Ta , $\text{B}=\text{Sc}$ or Zr). *Solid State Ionics* **282**, 7–12.
22. Murugan, R., Thangadurai, V., and Weppner, W. (2007). Fast lithium ion conduction in garnet-type $\text{Li}_7\text{La}_3\text{Zr}_2\text{O}_{12}$. *Angew. Chem. Int. Ed. Engl.* **46**, 7778–7781.
23. Duan, H., Zheng, H., Zhou, Y., Xu, B., and Liu, H. (2018). Stability of garnet-type Li ion conductors: an overview. *Solid State Ionics* **318**, 45–53.
24. Farley, T.W.D., Hayes, W., Hull, S., Hutchings, M.T., and Vrtis, M. (1991). Investigation of thermally induced Li^+ ion disorder in Li_2O using neutron diffraction. *J. Phys. Condens. Matter* **3**, 4761–4781.
25. Idemoto, Y., Richardson, J.W., Koura, N., Kohara, S., and Loong, C.K. (1998). Crystal structure of $(\text{Li}_{x}\text{K}_{1-x})_2\text{CO}_3$ ($x = 0, 0.43, 0.5, 0.62, 1$) by neutron powder diffraction analysis. *J. Phys. Chem. Solids* **59**, 363–376.
26. Wyckoff, R.W.G. (1963). *Crystal Structures Vol. 1*, Second edition (Interscience Publishers), pp. 239–444.
27. Ziv, B., Borgel, V., Aurbach, D., Kim, J., Xiao, X., and Powell, B.R. (2014). Investigation of the reasons for capacity fading in Li-Ion battery cells. *J. Electrochem. Soc.* **161**, A1672–A1680.
28. Son, S.B., Cao, L., Yoon, T., Cresce, A., Hafner, S.E., Liu, J., Groner, M., Xu, K., and Ban, C. (2019). Interfacially induced cascading failure in graphite-silicon composite anodes. *Adv. Sci.* **6**, 1801007.
29. Ellis, L.D., Hill, I.G., Gering, K.L., and Dahn, J.R. (2017). Synergistic effect of LiPF_6 and LiBF_4 as electrolyte salts in lithium-ion cells. *J. Electrochem. Soc.* **164**, A2426–A2433.

30. Kozen, A.C., Pearse, A.J., Lin, C., Schroeder, M.A., Noked, M., Lee, S.B., and Rubloff, G.W. (2014). Atomic layer deposition and in situ characterization of ultraclean lithium oxide and lithium hydroxide. *J. Phys. Chem. C* 118, 27749–27753.
31. Sun, J., Zhao, N., Li, Y., Guo, X., Feng, X., Liu, X., Liu, Z., Cui, G., Zheng, H., Gu, L., et al. (2017). A rechargeable Li-air fuel cell battery based on garnet solid electrolytes. *Sci. Rep.* 7, 41217.
32. Sharafi, A., Kazyak, E., Davis, A.L., Yu, S., Thompson, T., Siegel, D.J., Dasgupta, N.P., and Sakamoto, J. (2017). Surface chemistry mechanism of ultra-low interfacial resistance in the solid-state electrolyte $\text{Li}_7\text{La}_3\text{Zr}_2\text{O}_{12}$. *Chem. Mater.* 29, 7961–7968.